# Implications of Co-Feeding Water on the Growth Mechanisms of Retained Species on a SAPO-18 Catalyst during the Methanol-to-Olefins Reaction

José Valecillos,*[a] Idoia Hita,[b] Enrique Sastre,[c] Andrés T. Aguayo,[a] and Pedro Castaño*[a, b]

The dynamics of retained and deactivating species in a SAPO-18 catalyst during the methanol-to-olefins reaction have been followed using a combination of *ex-situ* and *in-situ* techniques in differential and integral reactors.The retained species were analyzed using extraction, *in-situ* FTIR and *in-situ* UV-vis spectroscopies combined with online product analysis (gas chromatography and mass spectrometry). The composition of the extracted soluble species was determined using gas chromatography-mass spectrometry and that of the insoluble species using high-resolution mass spectrometry. We observe a decrease in the formation and degradation rates of retained species when co-feeding water, whereas the extent of the decreases is the same across the entire spectrum of retained molecules. This indicates that co-feeding water unselectively quenches the formation of active and deactivating species. At the same time, the catalyst has an extended lifetime when co-feeding water due to the diffusion of species (particularly olefins) out of the SAPO-18 crystals, and subsequent growth of heavy polycyclic aromatic structures that imply less deactivation. These conclusions can be extrapolated to other MTO catalysts with relatively similar pore topology such as SAPO-34 or SSZ-13 structures.

## 1. Introduction

The catalytic conversion of methanol to olefins (MTO) is a promising alternative for the production of petrochemicals. The common catalyst for the development of the MTO process is based on the SAPO-34 zeotype (CHA structural topology).[1–5] However, alternative catalysts based on the SAPO-18 zeotype (AEI structural topology) show promising kinetic results with an improved selectivity towards propylene and butylenes,[2,6–12] and prolonged catalyst lifetime.[13] Both zeotypes belong to the family of small-pore openings (8-membered rings) with large cavities differing in shape, offering a strong shape selectivity that is beneficial for a high selectivity of short-chain olefins but detrimental for a rapid formation and accumulation of coke that leads to fast catalyst deactivation. The difference in the cavities, which affects the diffusion of molecules, may be responsible for improving the selectivity of propylene and butylenes.[14,15] The MTO reaction on SAPO-18 catalysts follows the well-established dual-cycle mechanism,[16–19] comprising an olefins and aromatics cycle. The hydrocarbon pool of olefinic and aromatic species undergoes reactions of methylation of olefins or aromatics, dealkylation of alkylaromatics, oligomerization of olefins, cracking of olefins, cyclization of olefins and hydrogen transfer between aliphatic and cyclic olefins. Methane is another relevant byproduct of the MTO reaction and its formation occurs by (i) thermal decomposition of oxygenates, or (ii) hydrogen abstraction from a hydrocarbon pool species to a surface methoxide species.[20,21]

In SAPO-18 and -34 catalysts, the aromatic pool species remain trapped in the cavities (as the openings are smaller than the benzene molecule, being this the smallest aromatic species). This gives rise to coke formation through the degradation of hydrocarbon pool species into bulky aromatics constraining the diffusion of methanol and olefins.[22–28] The *in-situ* or *ex-situ* analyses of retained species reveal the presence of mono-, bi-, tri- and tetracyclic aromatics remaining in the catalyst during or after the MTO reaction (which are soluble in organic solvents and therefore these species are often referred to as soluble species).[6,17,24,29–35] There are many research works on the MTO reaction using *in-situ* or *operando* spectroscopies to study the retained species in the catalyst, particularly ultraviolet-visible (UV-vis) spectroscopy[24,33,34,36–39] and Fourier transform infrared (FTIR) spectroscopy.[24,33,39] The challenge is to apply these techniques together with the analysis of products to correlate both active species with kinetics and deactivation, which could be instrumental to solve the fate of the hydrocarbon pool species.[40]

[a] Dr. J. Valecillos, Prof. A. T. Aguayo, Dr. P. Castaño
Department of Chemical Engineering
University of the Basque Country (UPV/EHU)
P.O. Box 644
Bilbao, 48080 (Spain)
E-mail: jose.valecillos@ehu.eus
[b] Dr. I. Hita, Dr. P. Castaño
Multiscale Reaction Engineering
KAUST Catalysis Center (KCC)
King Abdullah University of Science and Technology (KAUST)
Thuwal, 23955-6900 (Saudi Arabia)
E-mail: pedro.castano@kaust.edu.sa
[c] Prof. E. Sastre
Instituto de Catálisis y Petroleoquímica (CSIC)
C/Marie Curie, 2
28049 Madrid (Spain)

Olefins and monocyclic aromatics are normally active species depending on the shape and size of cavities,[14,15] whereas bicyclic aromatics may be either active or deactivating species depending on the reaction conditions for SAPO-34 catalysts.[34] Interestingly, Zhou et al.[41] found that a pre-coked SAPO-34 catalyst turned out to be active for the MTO reaction with improved ethylene selectivity, being bicyclic aromatics active for the ethylene formation. Other research works have demonstrated the formation of larger (and insoluble) polycyclic aromatics in small-pore catalysts, which have been hypothesized to be on the external surface of the crystal[25] or forming cross-cavity polycyclic aromatic species at the edge of the crystal.[42] In two recent works from Liu and co-workers,[43,44] the nature of the coke species have been revealed using Fourier transformed ion cyclotron resonance (FT-ICR/MS). These works indicate, for the first time, that coke growths in SAPO-18 or -34 following a cage-passing mechanism, cross-linking multicore aromatics.

The rapid coke formation during MTO has been circumvented combining two strategies:[1,45–48] (i) using a circulating fluidized-bed reactor (inspired in the fluid catalytic cracking reactor), and (ii) diluting the methanol feed with water for alleviating catalyst deactivation and removing the reaction heat in the MTO reaction. The latter strategy has also been proved to be positive for the MTO reaction on SAPO-18 catalysts from an experimental point of view.[10,20,49] In general, water is regarded as an agent that inhibits the formation of hydrocarbon pool species delaying the induction-autocatalytic period, and the degradation of these into coke leading to attenuated catalyst deactivation.[42] These observations are compatible with the competitive adsorption among methanol, olefins and water, in which water is strongly chemisorbed and hence decreasing the availability of acid sites and favoring the suppression of coke formation.[50] De Wispelaere et al.[51] carried out molecular dynamics simulations and *in-situ* microspectroscopy with the purpose of deepening the insights into the effects of co-feeding water in the MTO reaction on SAPO-34 catalysts. Besides the known effect of competitive adsorption, they found that water lowers the reactivity of methanol to form surface methoxide species as water molecules are less efficient protic molecules for assisting this reaction. The low reactivity of methanol leads to slowing down the formation of bulky hydrocarbon pool species, which alleviates the diffusional limitations of methanol and olefins for reaching the inner cavities of the crystal. They concluded that all these effects translate into an enhanced use of the SAPO-34 crystals, and hence more methanol and olefins can reach the inner cavities and eventually more hydrocarbon pool species and coke are formed. Very similar behavior has been observed for SAPO-34 crystals with low acidity.[44]

In this work, we have explored the effect of co-feeding water in the MTO reaction on a SAPO-18 catalyst for the MTO process. We adjusted the concentration of water and inert diluent in the feed with the purpose of obtaining different water-to-methanol ratio values in the feed at a constant methanol partial pressure. Our experimental approach consists of using three reaction systems comprising *in-situ* UV-vis and FTIR cell differential reactors, operating at low conversion and tracking the spectroscopic signatures of retained species that are incipiently formed, and a fixed-bed integral reactor in which we can reach the entire regime of conversions. We carried out a preliminary kinetic analysis in the cell reactors running experiments with pure methanol and methanol-water feeds for an identical duration to determine how co-feeding water affects the conversion rate of oxygenates and the formation rate of retained species. Afterwards, we carried out a deactivation analysis in the fixed-bed reactor running experiments with methanol and methanol-water feeds for different durations up to a similar final conversion level and therefore obtaining a severely deactivated catalyst to determine how co-feeding water affects the species retained in the catalyst at a severe deactivation state. In all cases, we analyzed in detail the products together with the retained species (soluble retained species extraction, temperature-programmed desorption or oxidation and, in *in-situ* spectroscopies in the cell reactors). We also examined the insoluble retained species using high resolution mass spectrometry (FT-ICR/MS). Our combined analytical/spectroscopic approach aims to uncover the intrinsic effect of water on the formation of active species and their degradation into deactivating ones. In other words, we intend to analyze if water can benefit more the reaction than the deactivation.

## 2. Results and Discussions

### 2.1. Catalyst Characterization

The catalyst used contains 50 wt% of SAPO-18 zeotype, 30 wt% of boehmite and 20 wt% of $\alpha$-alumina. The main observations for the zeotype and catalyst characterization are:

(i) The elemental composition analysis using XPS (Table 1) indicates that the SAPO-18 zeotype has a nominal Si/(Al + P) atomic ratio of 0.444.

**Table 1.** Main properties of the SAPO-18 zeotype and catalyst.

| | Si/(Al + P) [mol mol$^{-1}$] | $S_{BET}$ [m$^2$ g$^{-1}$] | $S_{micro}$ [m$^2$ g$^{-1}$] | $C_S$ [μmol g$^{-1}$] | $C_{WAS}$ [μmol g$^{-1}$] | $C_{MAS}$ [μmol g$^{-1}$] | $C_{SAS}$ [μmol g$^{-1}$] |
|---|---|---|---|---|---|---|---|
| SAPO-18 zeotype | 0.444 | 628 | 591 | 718 | 61.0 | 262 | 395 |
| SAPO-18 catalyst | | 353 | 240 | 408 | 28.0 | 181 | 199 |

$S_{BET}$ = specific surface area based estimated using the BET method. $S_{micro}$ = specific surface area of micropores estimated using the t-plot method. $C_S$ = concentration of acid sites estimated from the $NH_3$ adsorption measurements. $C_{WAS}$, $C_{MAS}$, $C_{SAS}$ = concentrations of weak-strength acid sites (WAS), medium-strength acid sites (MAS) and strong-strength acid sites (SAS) estimated from the $NH_3$-TPD measurements.

(ii) The XRD patterns of the active phases (Figure 1a) show characteristic peaks with maxima at the indicated diffraction angles (2θ) for a AEI structure (SAPO-18 zeotype).[8,11,52] Furthermore, we verified the incorporation of Si atoms into the AlPO structure of the synthesized SAPO-18 zeotype using $^{29}$Si solid-state NMR (Figure 1b), indicating the presence of different $Si(OSi)_x(OAl)_y$ species. However, we infer that the degree of substitution is low on the basis that the band of $Si(OSi)_4$ species is more intense than the bands of $Si(OAl)_4$, $Si(OSi)(OAl)_3$, $Si(OSi)_2(OAl)_2$ and $Si(OSi)(OAl)_3$ species.

(iii) The SAPO-18 zeotype has a large microporous surface (Table 1), as expected. The corresponding final catalysts have a major mesoporous surface due to the presence of the added alumina phases,[53] which is expected to enhance the catalyst performance.

(iv) The adsorption of $NH_3$ at 150 °C indicates that the SAPO-18 zeotype has a high concentration of acid sites (Table 1). The dilution of the zeotype with the alumina phases to obtain the catalysts caused a decrease of the concentration of acid sites by about 43%. The acid strength determined using $NH_3$-TPD (Figure 1c) evidences a high presence of strong-strength acid sites in the zeotype. However, the distribution of acid sites by their strength decreases for the catalyst resulting in about 48% of strong-strength acid sites and 43% of medium-strength acid sites.

(v) The nature of acid sites, studied with the vibration of O–H bonds in the 3500–3800 $cm^{-1}$ region in the infrared spectrum (Figure 1d), comprises:[40] bridged Al–OH–Si contributing to Brønsted acid sites (3593 $cm^{-1}$), aluminols (~3672 $cm^{-1}$), P–OH species in the SAPO-18 catalyst (~3672 $cm^{-1}$), silanols (3716 and 3734 $cm^{-1}$), and aluminols of the added alumina phases (3761 $cm^{-1}$). The low intensity of the 3593 $cm^{-1}$ band agrees with the low incorporation of Si atoms in the AlPO structure. On the other hand, the narrow and intense band at 3672 $cm^{-1}$ indicates the presence of P–OH species that are inferred to account for the high concentration of acid sites and acid strength.

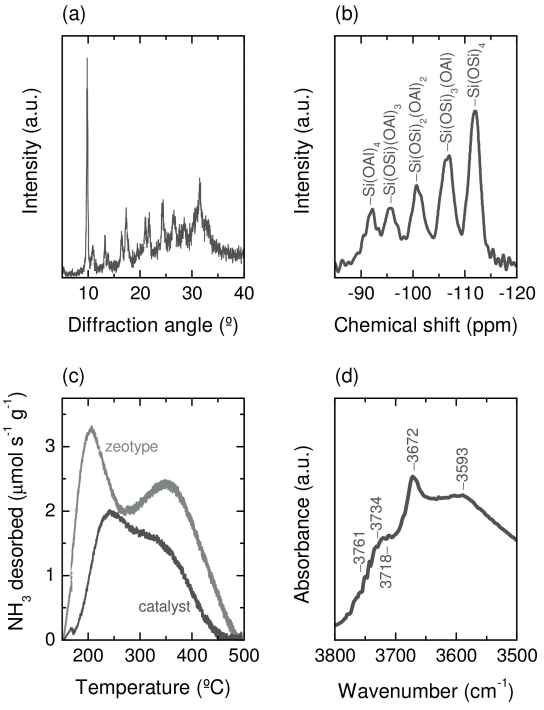


**Figure 1.** Main characterization results of the fresh catalyst used in this work: (a) XRD pattern of the synthetized SAPO-18 zeotype; (b) $^{29}$Si NMR spectrum of the synthetized SAPO-18 zeotype; (c) $NH_3$-TPD profiles for the SAPO-18 zeotype and catalyst; (d) FTIR spectrum in the 3500–3800 $cm^{-1}$ region at 400 °C of the SAPO-18 catalyst.

### 2.2. Kinetic Analysis in a UV-vis Cell Reactor

Firstly, we analyzed the effect of co-feeding water on the MTO reaction performance carrying out experiments in a UV-vis cell reactor at low methanol partial pressures, low catalyst loadings and identical duration (240 min). The use of a UV-vis cell reactor provides fundamental kinetic insights based on the simultaneous analyses of the gaseous effluent and the formation of retained species on the catalyst surface detected using UV-vis spectroscopy. Likewise, the use of low methanol partial pressures is beneficial for controlling the reaction rates of each kinetic period and, therefore, observing the incipient formation of retained species. This section presents the results for the online analysis of gaseous products and *ex-situ* analysis of retained species (at the end of each experiment), and the additional *in-situ* analysis of retained species by means of UV-vis spectroscopy.

#### *2.2.1. Ex-situ Analysis of Products*

Figure 2a shows the evolution with time on stream of the conversion for the MTO reaction on a SAPO-18 catalyst in the UV-vis cell reactor at water-to-methanol ($F_{W0}/F_{M0}$) ratio values in the feed of 0 and 0.50 while keeping constant the methanol partial pressure ($P_{M0}$ = 0.014 bar). As seen, the conversion increases reaching a maximum and then decreases upon increasing the time on stream for both experiments. These conversion profiles evidence the presence of (1) an induction-autocatalytic period, commonly reported in the literature,[10,20,49,54] in which the conversion increases with increasing time on stream up to reaching a maximum value, followed by a (2) deactivation period, in which the conversion decreases with increasing time on stream. The induction-autocatalytic period is suggested to be dominated by an olefin cycle on SAPO-34 catalysts[55] (relatively similar to that of SAPO-18 catalyst), in which olefins are formed through the methylation of olefins and subsequent cracking reactions, and cyclization and hydrogen transfer reactions forming aromatics. The conversion profiles evidence that co-feeding water slows down the kinetics of all the periods and lowers the maximum conversion that can be reached in the induction-autocatalytic period. This is concluded from the slopes at the period in which the conversion increases with increasing time on stream (induction-autocatalytic period) and at which the conversion

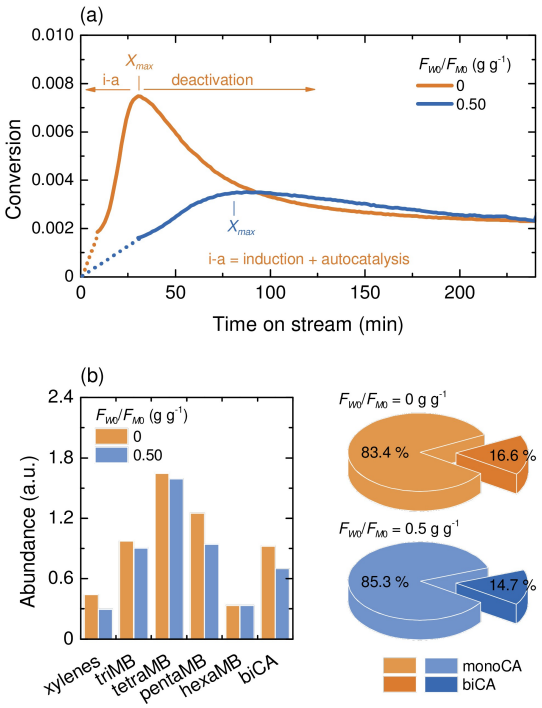


**Figure 2.** Effect of co-feeding water on the (a) conversion for the MTO reaction on a SAPO-18 catalyst in the UV-vis cell reactor, $T = 400\,^{\circ}C$, $P_{M0} = 0.014$, $W/F_{M0} = 1$ g h mol$^{-1}$, $F_{W0}/F_{M0} = 0$–0.5; and (b) distribution of coke soluble species after the MTO reaction in the UV-vis cell reactor using the conditions indicated before. Abbreviations: CA = cyclic aromatics, MB = methylbenzene.

decreases with increasing time on stream (deactivation period). Both slopes are noticeably smaller for the experiment with water co-feed than for the experiment with a pure methanol feed. The effect of co-feeding water on the kinetics for our SAPO-18 catalyst is similar to the observations for ZSM-5 catalysts,[56] in which the competitive adsorption of water decreases the available acid sites for the reaction (leading to decrease the density of acid sites at the reaction conditions).

After each experiment in the UV-vis cell reactor (same reaction duration), we analyzed the spent catalysts carrying out the extraction of retained species with dichloromethane. The main identified products were xylenes, tri-, tetra-, penta- and hexamethylbenzenes, and polymethylnaphthalenes, all of them soluble in dichloromethane with no evidence of insoluble species. Figure 2b shows a detailed distribution of the monocyclic aromatic species (bar chart) and the relative distribution between monocyclic and bicyclic aromatic species (pie charts) for the feeds of pure methanol and methanol-water. As seen, co-feeding water lowers the content of soluble species that can be detected at the end of the reaction (same reaction duration), with a similar effect for all the components in the hydrocarbon pool. These results also provide a direct observation on the average formation rate of soluble species since both spent catalysts were obtained at the same time on stream (240 min). Thus, we can also verify that co-feeding water lowers the average formation rate of soluble species.

### 2.2.2. In-situ Analysis by UV-Vis Spectroscopy

At the same time, we collected UV-vis spectra of the catalyst under working conditions every 35 s. Figure 3 shows the evolution with time on stream of these spectra for the experiments with water-to-methanol ratio values in the feed of 0 and 0.50. As seen, various UV-vis bands (indicated in the figure) rise upon exposing the catalyst to feeds of methanol or methanol-water, which are related to the formation of retained hydrocarbon species (π-π* transitions). The 388 nm band is the first to rise and its intensity continues to grow with increasing time on stream while another important band rises at 290 nm. At the maximum conversion (indicated by the highlighted spectrum at 30.3 and 82.0 min for feeds of methanol or methanol-water, respectively), the band at 388 nm is apparently broadened by the appearance of bands at 410 and 434 nm. These bands are commonly assigned to neutral aromatics (for the 290 nm band), and either olefin or alkylbenzene carbocations (for the bands in the 388–434 nm range).[31,34,55] Likewise, other bands grow up slowly at 500 and 616 nm, indicating the formation of more developed polycyclic aromatics.[31,34] Thus, presumably, olefins are formed first and after certain time on stream the appearance of aromatics is evidenced with the band rising at 290 nm and the progressive growth of the 388–434 nm bands. The comparison of Figure 3a (pure methanol feed) and Figure 3b (methanol-water feed) evidences that co-feeding water delays the evolution with time on stream of the intensities of all the bands.

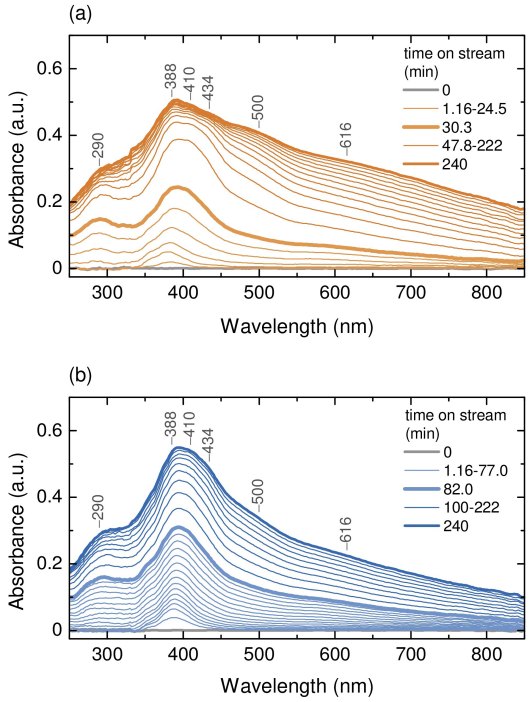


**Figure 3.** Effect of co-feeding water on the evolution with time on stream of the UV-vis spectra in the MTO reaction on a SAPO-18 catalyst: (a) $F_{W0}/F_{M0} = 0$; (b) $F_{W0}/F_{M0} = 0.50$. Spectra data represented at intervals of 350 s (5.83 min) from zero to the time on stream of maximum conversion (indicated for each experiment) and afterwards at intervals of 1050 s (17.5 min) until 240 min.

Since the collection of spectra at short intervals of time (35 s) gives enough kinetic data, we calculated the formation rate of the most relevant bands and plotted the results against time on stream. Figure 4 shows the results for these calculations, indicating that all the bands including 388, 500 and 616 nm (Figures 4a, 4b and 4c, respectively) show similar steps of induction-autocatalytic and deactivation periods, as previously showed in Figure 2a for the conversion. We can approximate the assignations of these bands to different monocyclic (388 nm) and bicyclic aromatic species (500 and 616 nm),[44] as only these species were detected within the soluble species with no evidence of insoluble species. However, we acknowledge that this assignation is not absolute as olefin carbocations cannot be easily distinguished from aromatic carbocations in the UV-vis spectrum. Thus, in the first period, the formation rate of monocyclic and bicyclic aromatics reaches a maximum[57,58] at a time on stream that coincides with that of the maximum conversion. That is, the formation rate corresponds to the formation of hydrocarbon pool species based on carbocations of aromatics or olefins that act as co-catalytic sites. In the deactivation period, the formation rate decreases with increasing time on stream indicating the catalyst deactivation. The kinetic behavior of the 500 and 616 nm bands also comprises two periods corresponding to the autocatalytic and deactivation stages. The formation rate decreases with increasing time on stream, but it does not clearly tend to zero, indicating a continuous coke formation, particularly in the case of co-feeding water. Co-feeding water notably slows down the formation of the species participating in all the periods, as previously evidenced in Figure 3 and in correspondence with the conversion profiles (Figure 2a). At the same time, co-feeding water lowers the maximum formation rate of the three species detected using UV-vis spectroscopy in analogy with the decrease in the maximum conversion (Figure 2a). Thus, the kinetics of the conversion of oxygenates and the formation of retained species are correlated and equally affected by the presence of high water concentrations when co-feeding water. These observations confirm the previously mentioned effects of water on lowering the density of acid sites (by the competitive adsorption of water on acid sites). We compared the quenching effect (Eq. (1)) of co-feeding water on the formation rate of the species detected using UV-vis spectroscopy, and we applied this calculation over the entire range of wavelengths.

$$\xi_{0.5} = \frac{[r_{max}]_{0.5}}{[r_{max}]_0} \quad (1)$$

A value of $\xi = 0$ would mean that co-feeding water completely depletes the formation rate, $\xi = 1$ would mean that co-feeding water does not affect the formation rate, $0 < \xi < 1$ would mean that co-feeding water slows down the formation rate at different degrees and $\xi > 1$ would mean co-feeding water accelerates the formation rate. Figure 4d shows the extent of the quenching effect of co-feeding water ($\xi$) as a function of the wavelengths in the UV-vis spectrum. As seen in this graph, all values of $\xi$ lie in a narrow range 0.34–0.44 (for wavelengths higher than 700 nm the errors are relatively high due to the negligible formation of the species that absorb in this region). That is, co-feeding water quenches in a 56–66% extent the formation rates of all the retained species absorbing in the range 250–700 nm. Interestingly, this result points out that co-feeding water does not affect the net growth of active species (typically $\leq$388 nm) as compared to that of the deactivating species ($\geq$500 nm).

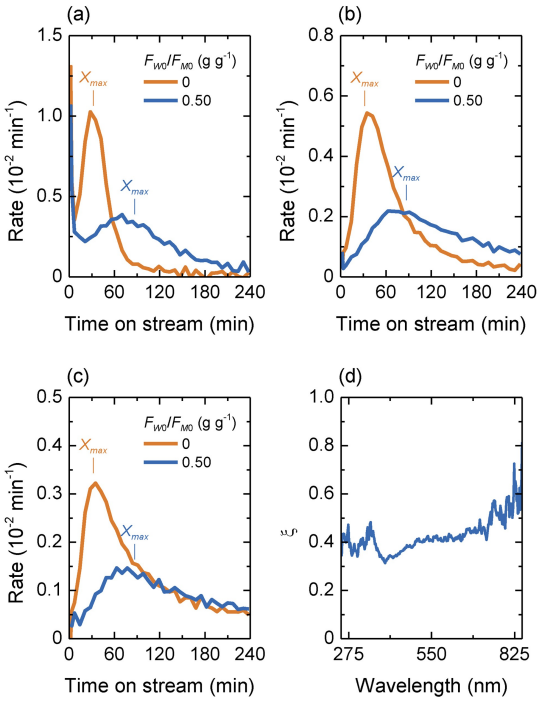


**Figure 4.** Effect of co-feeding water on the evolution with time on stream of the maximum intensity of UV-vis bands in the MTO reaction on a SAPO-18 catalyst in a cell reactor: (a) 388 nm; (b) 500 nm; (c) 616 nm. These bands can be assigned (approximately) to monocyclic and bicyclic aromatics.
(d) Quenching effect ($\xi$) of co-feeding water on the formation rate of species detected in the whole UV-vis spectrum.

### 2.3. Kinetic Analysis in a FTIR Cell Reactor

The *in-situ* formation of retained species was also monitored using FTIR spectroscopy in a FTIR cell reactor. The experimental variables were similar to the previous ones used for the UV-vis cell reactor. This section presents the results for the online analysis of gaseous products, and the *in-situ* and *ex-situ* analysis of retained species. Our main goal is to analyze the quenching effect of co-feeding water on the formation rate and nature of retained species that can be detected using FTIR spectroscopy.

#### *2.3.1. Ex-situ Analysis of Products*

Figure 5a shows the evolution with time on stream of the conversion for the MTO reaction on the SAPO-18 catalyst in the FTIR cell reactor at water-to-methanol ($F_{W0}/F_{M0}$) ratio values of 0 and 0.50 while keeping constant the methanol partial pressure

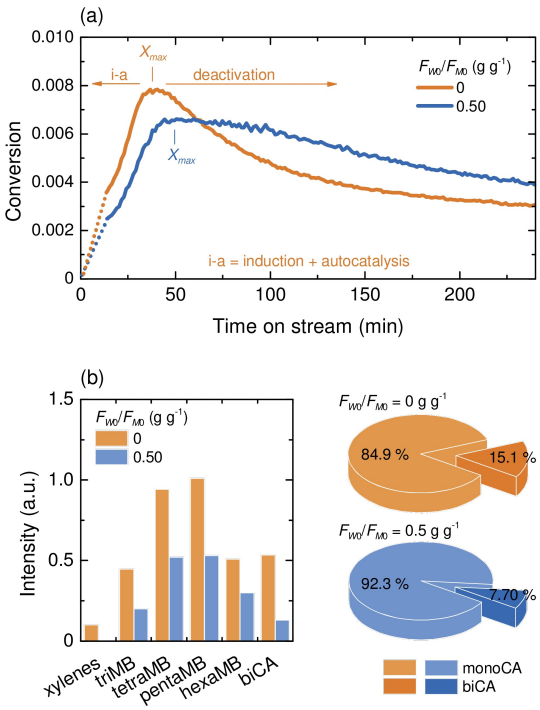


**Figure 5.** Effect of co-feeding water on the (a) conversion for the MTO reaction on a SAPO-18 catalyst in the FTIR cell reactor, $T = 400\,^{\circ}C$, $P_{M0} = 0.014$, $W/F_{M0} = 1$ g h mol$^{-1}$, $F_{W0}/F_{M0} = 0$–0.5; and (b) distribution of coke soluble species after the MTO reaction in the FTIR cell reactor using the conditions indicated before. Abbreviations: CA = cyclic aromatics, MB = methylbenzene.

($P_{M0} = 0.014$ bar). As seen, the conversion profiles exhibit the three kinetic periods previously observed for the experiments in the UV-vis cell reactor, clearly evidencing the periods of induction-autocatalysis and deactivation. The results indicate once again that co-feeding decreases the maximum conversion observed in the induction-autocatalytic period and slows down the kinetics of all the periods. The latter observation is based on the graphical slopes at the induction-autocatalytic period (the conversion increases with increasing time on stream) and at the deactivation period (the conversion decreases with increasing time on stream). These results particularly indicate that co-feeding water attenuates catalyst deactivation by substantially slowing down the decrease in the conversion (much smaller slope) during the deactivation period for the methanol-water feed. The fact that both maxima are reached at almost the same time on stream (with and without co-feeding water) as compared with the UV-vis cell reactor, indicates that the contact between the catalyst and the gaseous phase is quite different in both cell reactors due to their different geometries. Thus, a further study is required in this sense. Here, we compare only the net effect of water on the quenching effect of co-feeding water on the formation rates and the nature of the retained species.

After the experiments in the FTIR reactor, we analyzed the spent catalysts carrying out extraction of species with dichloromethane. The main identified species were similar to those observed in the experiments in the UV-vis cell reactor (soluble species), with no evidence of insoluble species. Figure 5b shows a detailed distribution of the monocyclic aromatic species (bar chart) and the relative distribution between monocyclic and bicyclic aromatic species (pie charts) for the feeds of pure methanol and methanol-water. As seen, co-feeding water decreases the content of soluble species that can be detected at the end of the reaction with a similar effect for all the components. The results of Figure 5b can directly provide information on the average formation rate of soluble species as the spent catalyst were obtained at equal experiment duration (240 min). Thus, we can verify that co-feeding water slows down the average formation rate of soluble species.

### 2.3.2. In-situ Analysis by FTIR Spectroscopy

Figure 6 shows the evolution with time on stream of FTIR spectra taken during the MTO reaction at intervals of 10 min. As seen, various UV-vis bands (indicated in the figure) rise upon exposing the catalyst to feeds of pure methanol or methanol-water in the regions of stretching vibrations of O–H ($\upsilon_{O\text{-}H}$), C–H ($\upsilon_{C\text{-}H}$) and C=C ($\upsilon_{C=C}$) bonds and bending vibrations of C–H ($\delta_{C\text{-}H}$) and O–H bonds ($\delta_{O\text{-}H}$). These bands indicate (i) the formation of hydrocarbons that can be adsorbed on the entire catalyst surface (micro-, meso- and macropores) or in the gaseous phase; (ii) the adsorption of methanol or dimethyl ether (methoxy species) and water; (iii) the perturbation of acid sites by the adsorption of hydrocarbons and methanol. In general, the bands in the $\upsilon_{C\text{-}H}$ and $\upsilon_{C=C}$ bond regions present less

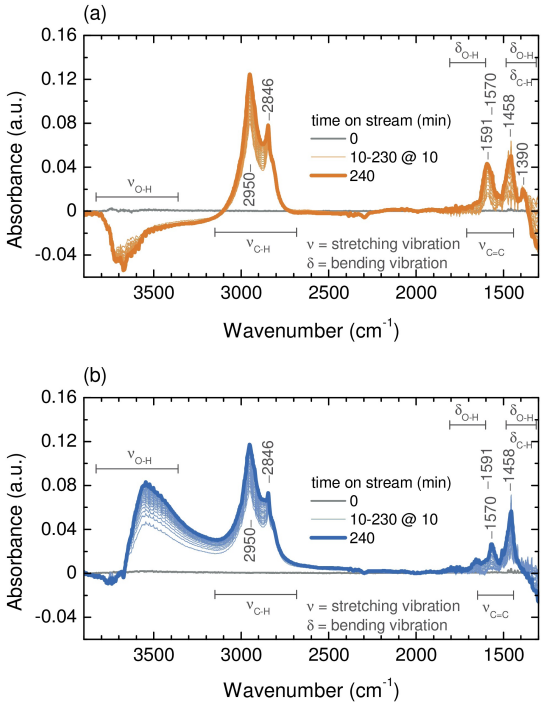


**Figure 6.** Effect of co-feeding water on the evolution with time on stream of the FTIR spectra in the MTO reaction on a SAPO-18 catalyst: (a) $F_{W0}/F_{M0} = 0$; (b) $F_{W0}/F_{M0} = 0.50$. Spectra data represented at intervals of 10 min.

absorbance intensities for the feed of methanol-water, whereas the bands in the $\upsilon_{O\text{-}H}$ and $\delta_{O\text{-}H}$ regions are more intense due to the high water concentration in the reaction medium. In a previous works,[40,59] we observed that the bands in the $\upsilon_{C=C}$ and $\delta_{C\text{-}H}$ regions are more reliable to study the retained species as they are less affected by gaseous phase or physisorbed species. The results clearly show that these bands (representative of retained species) are less intense for the feed of methanol-water, indicating that co-feeding water disfavors the formation of retained species as also observed in the experiments carried out using UV-vis spectroscopy.

Interestingly, the intensity of the 1390 ($\delta_{C\text{-}H}$) and 1591 ($\upsilon_{C=C}$) $cm^{-1}$ bands decreases so much for the methanol-water feed that it seems to be practically absent, whereas the 1570 $cm^{-1}$ band becomes more dominant in the region of retained species. According to the literature,[59,60] the simultaneous rise of the 1390 and 1591 $cm^{-1}$ bands can be related to absorbed olefins. The presence of olefins within the retained species in SAPO-34 catalysts was demonstrated using Raman spectroscopy by Rojo-Gama et al.,[61] being a finding applicable to our results since the SAPO-18 structure is relatively similar to that of SAPO-34. In contrast with UV-vis spectroscopy, Raman and FTIR spectroscopies allow to distinguish the aromatic or olefin nature of retained species, and with the latter technique we are able to confirm the abundant presence of olefins within the retained species in the SAPO-18 catalyst in particular for the experiment with a pure methanol feed. On the other hand, the 1570 $cm^{-1}$ band is related to retained species with an aromatic nature (presumably monocyclic and bicyclic aromatics as indicated by the analysis of soluble species). Thus, we infer that co-feeding water hinders the adsorption of olefins giving rise to a pool of retained species rich in aromatics. By representing the maximum intensity of the 1570 (aromatics) and 1591 (olefins) $cm^{-1}$ bands against the time on stream between 10 and 240 min on stream, we observed an approximate linear trend and thus we can estimate a constant formation rate of these bands throughout the experiments. The 1570 $cm^{-1}$ band is formed at a rate of 0.00734 and 0.00574 $h^{-1}$ for the pure methanol and methanol-water feeds, respectively. Likewise, the formation rate of the 1591 $cm^{-1}$ band is 0.00754 and 0.00207 $h^{-1}$ for the pure methanol and methanol-water feeds, respectively. These numbers demonstrate that the adsorption of olefins is more affected when co-feeding water than the formation and retention of aromatics.

By comparing the spectra dataset for both experiments in the $\upsilon_{O\text{-}H}$ region, it is also evident that the acid sites result less perturbed when co-feeding water. The spectra datasets further evidence that the adsorption of water (broad band towards 3500 $cm^{-1}$) may be responsible for the low formation of retained species in agreement with the statements of the literature. This also evidences that the adsorption of water hinders the adsorption of olefins, as reported for a SAPO-34 catalyst,[42] with a similar structure to the SAPO-18 catalyst.

### 2.4. Kinetic Results in a Fixed-Bed Reactor

The use of a fixed-bed reactor provides practical kinetic information with a detailed analysis of products for the effect of co-feeding water on the MTO reaction performance at relevant reaction conditions (high methanol partial pressure and catalyst load, and different experiment duration in comparison to the conditions used in the cell reactors). The use of a model reactor gives way to study a wide range of conversions with severe states of catalyst deactivation (high levels of coke formation) with more possibilities to use powerful *ex-situ* techniques to analyze the effect of co-feeding water on the nature of retained species. We intentionally varied the duration of the experiments with the purpose of obtaining severely deactivated catalysts at a similar final conversion value (around 3%). This section presents the results for a more detailed online analysis of gaseous products and *ex-situ* analysis of retained species.

#### *2.4.1. Online Analysis of Products*

Figure 7 shows the evolution with time on stream of the conversion for the MTO reaction on a SAPO-18 catalyst in a fixed-bed reactor at different water-to-methanol ($F_{W0}/F_{M0}$) ratio values in the feed and different experiment duration while keeping constant the methanol partial pressure ($P_{M0}=0.61$ bar). As seen, the catalyst undergoes very rapid deactivation from the beginning of the reaction as indicated by the rapid decrease of the conversion with increasing time on stream, which does not allow determining an initial, maximum or steady-state conversion value for each experiment. The limitations for measuring initial kinetic data in laboratory reactors using similar catalysts (e.g. SAPO-34) with very fast deactivation is a fact acknowledged in the literature.[26] However, using low loadings of catalyst (low space time values) on purpose leads to obtaining low conversion levels throughout the catalyst lifetime, which is an appropriate regime to study differences in the kinetic performances under variable reaction parameters (e.g. varying the feed composition co-feeding water). The conversion

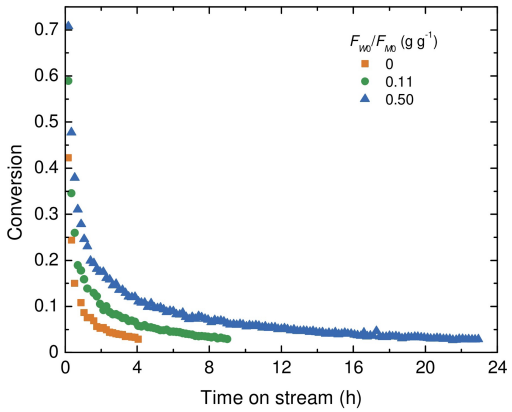


**Figure 7.** Effect of co-feeding water on the conversion profiles for the MTO reaction on a SAPO-18 catalyst in a fixed-bed reactor. Conditions: $T=400\,°C$, $P_{M0}=0.61$, $W/F_{M0}=1$ g h mol$^{-1}$, $F_{W0}/F_{M0}=0$–0.5.

profiles indicate that co-feeding water substantially slows down the rate at which the conversion decreases, graphically evidenced with the different slopes at which the conversion decreases with time on stream up to reaching a similar final conversion value. As a result, co-feeding water prolongs catalyst lifetime, and increasing the water-to-methanol ratio in the feed enhances this effect. From the dataset, the catalyst lifetime (defined as the time on stream at which the conversion decreases down to 3%) is 4, 9 and 21 h for the experiments with water-to-methanol ratio values of 0, 0.11 and 0.50, respectively. Our observation agrees with that reported by Gayubo et al.[10,20] for a SAPO-18 catalyst, who concluded that water is an agent that inhibits the formation of hydrocarbon pool species and, more importantly, the evolution of these species into coke.

The species observed in the effluent gas were unreacted methanol, dimethyl ether, water, methane, carbon oxides and a mixture of aliphatic hydrocarbons, being a typical product distribution for the MTO reaction on SAPO-18 catalysts.[8,10,12,49,52] Figure 8 shows the evolution with the conversion of the selectivity of methane and aliphatic hydrocarbons grouped as light olefins ($C_2$-$C_4$), heavy aliphatics ($C_{5+}$ olefins and paraffins) and light paraffins ($C_2$-$C_4$). As seen, the selectivity of light olefins and heavy aliphatics remains invariable at high conversion values for all the experiments, whereas that of light olefins decreases and that of methane and heavy aliphatics increases at low conversion values. Co-feeding water notably increases the selectivity towards light olefins while decreases the selectivity towards methane and heavy aliphatics at low conversion values. The light paraffins selectivity is very low, almost zero for the experiment with a feed of pure methanol. However, the light paraffins selectivity increases for the experiments with water co-feed at high conversion values (beginning of the reaction), and then progressively decreases with decreasing conversion. The presence of light paraffins in the effluent gas may be an indicative of the formation of aromatics retained in the SAPO-18 cavities through cyclization and hydrogen transfer reactions.[12] Contrariwise, the absence of light paraffins in the effluent gas for the feed of pure methanol suggests that both hydrocarbon pool and coke species are immediately formed at the beginning of the reaction, causing the faster catalyst deactivation. In this case, the rate of cyclization and hydrogen transfer reactions is much faster and active at the very initial stage of the reaction (that is not captured in this experiment because of the rapid catalyst deactivation at the tested conditions), and these reactions are rapidly ceased due to the rapid blockage of cavities (according to the fast catalyst deactivation) hindering the diffusion of reactive species.

In general, the methane selectivity is low (almost zero) at the beginning of the reaction and increases with decreasing conversion values. The selectivity of methane decreases with increasing water-to-methanol ratio in the feed, being similar to the observations of Gayubo et al.[49] The methane formation in the MTO reaction on SAPO-18 or SAPO-34 catalysts is mainly attributable to the release from surface methoxide species by hydrogen abstraction from a hydrocarbon molecule (likely a component of hydrocarbon pool species), whereas the route of thermal decomposition of oxygenates is more significant at high temperatures (above 400 °C).[20,21] This indicates that the kinetic behavior for the formation of olefins should be linked with that of methane, and our results verify such trend: the selectivity of light olefins decreases while that of methane increases at low conversion values. Additionally, our results also verify that the decomposition of oxygenates should be negligible at the reaction temperature used in our experiments (400 °C), based on the low carbon dioxide selectivity (less than 2% in all the experiments). Thus, increasing the water-to-methanol ratio in the feed leads to disfavor the methane formation through the hydrogen abstraction from hydrocarbon pool species by surface methoxide species. The hydrogen abstraction from large hydrocarbon pool species may favor the coke formation,[21] and therefore the low methane formation is

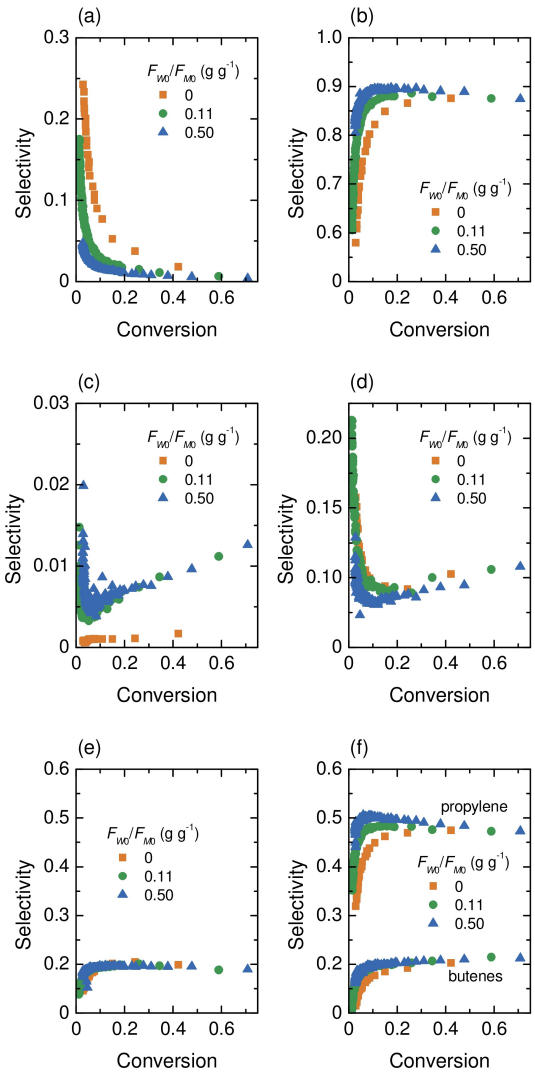


**Figure 8.** Effect of co-feeding water on the selectivity of the main lumps of products for the MTO reaction on a SAPO-18 catalyst in a fixed-bed reactor: (a) methane; (b) light olefins; (c) light paraffins; (d) $C_{5+}$ olefins; (e) ethylene; (f) propylene and butylenes. Conditions: $T = 400$ °C, $P_{M0} = 0.61$, $W/F_{M0} = 1$ g h mol$^{-1}$, $F_{W0}/F_{M0} = 0$–0.5.

an indicative of the advantage of co-feeding water to slow down the coke formation resulting in a prolonged catalyst lifetime.

To further investigate the effect of co-feeding water on the light olefins selectivity, Figure 8 also shows a detailed distribution of ethylene, propylene and butylenes for all the experiments. As seen, the selectivity of propylene is about twice higher than that of ethylene or butylene while that of ethylene and butylenes are comparable for all the experiments, being similar to the observations of Chen et al.[18] Increasing the water-to-methanol ratio in the feed remarkably increases the propylene selectivity, and slightly increases the butylenes selectivity, whereas the ethylene selectivity remains invariable, in good agreement with the results reported by Gayubo et al.[10,20] These observations clearly indicate that increasing the water-to-methanol ratio in the feed favors the formation of propylene over ethylene and, to a lesser extent, the formation of butylenes over ethylene, whereas the formation of butylenes over propylene seems to be unaffected. Gayubo et al.[20] proposed a mechanism for the individual formation of ethylene, propylene and $C_{4+}$ olefins formed independently from the reaction between oxygenates and hydrocarbon pool species, and found that the kinetic coefficient for the formation of propylene is higher than that of butylenes and ethylene, which justified the favored propylene selectivity. In their kinetic model, the effect of co-feeding water is explained by introducing a hyperbolic expression that attenuates the rate of every kinetic step, including the formation of individual light olefins.[49] This kinetic term accounts for the competitive adsorption of water on acid sites and justifies that a portion of these sites becomes unavailable for the reaction as they are covered with water.[51]

### *2.4.2. Ex-situ Analysis of Retained Species*

To complete our analysis of products, we quantified and evaluated the nature of retained species in the spent catalysts having undergone severe deactivation with a similar final conversion value reached at different duration for each experiment. It should be highlighted that these analyses of retained species correspond to different durations of experiments, which may affect the quantification or nature of retained species. However, the comparison of the retained species at equal final conversion values provides a better context for assessing the isolated impact of co-feeding water, without conversion being an additional variable. It is known that, comparing the retained species formed in experiments with equal durations but different conversion levels may hinder the evaluation of the actual effect of co-feeding water.[65] The following subsections show the results for the *ex-situ* analysis of retained species using temperature-programmed desorption (TPD) and oxidation (TPO), and extraction of retained species with dichloromethane (the soluble species in dichloromethane are analyzed using GC-MS and the insoluble portion is analyzed using LDI FT-ICR/MS).

#### 2.4.2.1. TPD and TPO Measurements

Figure 9 shows the TPD and TPO profiles for all the spent catalysts. As seen, there are not substantial differences among the TPD or TPO profiles (using different proportions of co-fed water), suggesting that the thermal behavior of the retained species at TPD or TPO conditions is similar. The TPD profiles show that the species start to be thermally removed or decomposed at 350 °C with an apparent unique maximum at 510 °C for the experiment with a pure methanol feed, and 530 °C for both experiments with methanol-water feeds. Likewise, the TPO profiles show the combustion of the remaining species that were not removed during the TPD, with a unique and intense peak centered at 540 °C for all the experiments. Since the AEI topology imposes strong shape constrains, it is expected that most of the species are trapped within the SAPO-18 cavities, while it is possible to expect the formation of external coke species due to the presence of acid sites on the surface of the SAPO-18 crystals and the catalyst matrix composed of γ-alumina.[25,53]

Table 2 lists the content of the retained species removed during the TPD and TPO measurements ($C_{TPD}$ and $C_{TPO}$, respectively), together with the catalyst lifetime (t) and the final conversion (X(t)), for each experiment at different water-to-methanol ratio in the feed. Despite of the different duration of the experiments (needed for reaching a similar final conversion), the content of species removed during the TPD and TPO measurements is similar for all the experiments with only slight differences between feeding pure methanol or methanol-water. The expected slower formation rate of retained species (proven with our *in-situ* analyses) explains that, even for different durations of the experiments, the total content of species is similar for each experiment and seems to reach a saturation value. In agreement with our results, Qi et al.[66] observed that the coke content remained invariable at different water-to-methanol ratio values in the feed once the catalyst reached saturation by accumulation of coke at long time on stream, and

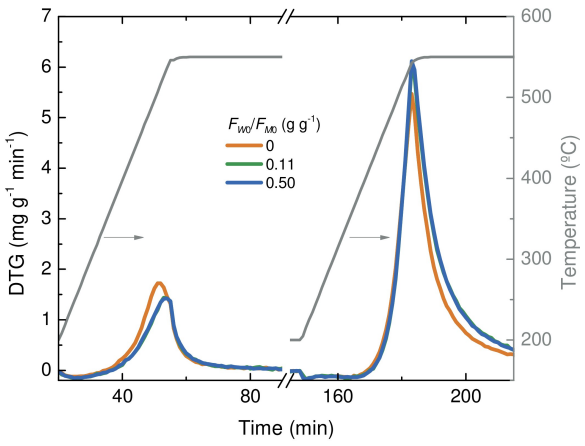


**Figure 9.** Effect of co-feeding water on the TPD and TPO profiles of the spent catalysts of the experiments performed in the fixed-bed reactor.

**Table 2.** Content of TPD and TPO species for the experiments performed in the fixed-bed reactor.

| Experiment | t [h] | X(t) | $C_{TPD}$ [mg g$^{-1}$] | $C_{TPO}$ [mg g$^{-1}$] | $C_{total}$ [mg g$^{-1}$] |
|---|---|---|---|---|---|
| $F_{W0}/F_{M0}=0$ | 4.0 | 0.0288 | 22.2 | 75.4 | 97.6 |
| $F_{W0}/F_{M0}=0.11$ | 9.0 | 0.0291 | 18.4 | 90.3 | 109 |
| $F_{W0}/F_{M0}=0.50$ | 23 | 0.0287 | 18.5 | 90.5 | 109 |

t = catalyst lifetime; X(t) = conversion at the catalyst lifetime; $C_{TPD}$ = content of TPD species; $C_{TPO}$ = content of TPO species; $C_{total}$ = total content of retained species.

the effect of co-feeding water on the coke content was no longer observed at such conditions.

As aforementioned, there is a slight difference in the content of retained species detected using TPD and TPO measurements between the experiments feeding pure methanol or methanol-water. Although the duration of the experiments is different (longer for the experiments feeding methanol-water), it is notorious that the content of retained species is slightly lower for the experiment without water co-feed than for those with water co-feed at the same conversion level. It is reasonably expected that longer experiments lead to the formation of higher amounts of retained species, but it is also expected that co-feeding water contributes to form more retained species in similar catalyst structures (SAPO-34 catalysts) as reported by De Wispelaere et al.[51] In their work, they observed an increase in the thickness of coke at the edge of a SAPO-34 crystal with increasing water concentrations in the reaction medium. They rationalized this observation based on the efficient use of the crystal when co-feeding water: in the experiment with a pure methanol feed, coke was rapidly formed in the cavities closer to the external surface blocking the diffusion of methanol and olefins to the inner cavities that remained empty (without retained species).

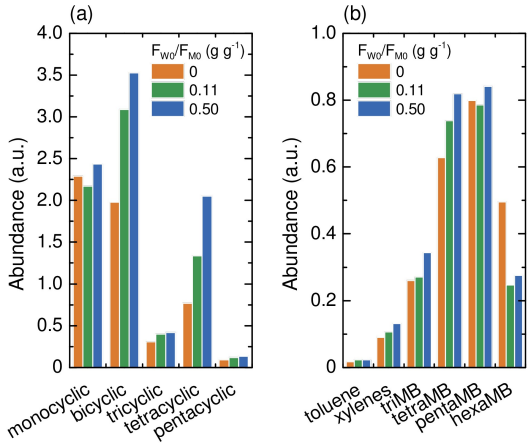


**Figure 10.** Effect of co-feeding water on the distribution of soluble retained species in the spent catalysts of the experiments performed in the fixed-bed reactor: (a) lumps of monocyclic and polycyclic aromatics and (b) components of monocyclic aromatics.

### 2.4.2.2. Analysis of Soluble Species

The extraction and characterization of retained species that are soluble in dichloromethane gave us additional clues on the chemistry of retained species. We observed that the extract contains soluble species in dichloromethane and insoluble species (black residue). The soluble species dissolved in dichloromethane were analyzed using GC-MS (the analysis of the insoluble species is presented in the next section). The main identified soluble species are monocyclic, bicyclic, tricyclic and tetracyclic aromatics, in agreement with the observations reported for SAPO-18 catalysts[67] and similar catalyst topologies.[23,25,68] It is expected to find olefins and monocyclic aromatics within the retained species that act as hydrocarbon pool species in SAPO-18 and SAPO-34 catalysts, whereas other polycyclic aromatics found are deactivating species (coke),[17,18,29,35,67,69] though bicyclic aromatics may also be hydrocarbon pool species in SAPO-34 catalysts depending on the temperature.[34]

Figure 10a shows the abundance of these species for each experiment. As seen, the abundance of monocyclic aromatics is similar for all the experiments, whereas the abundance of bicyclic, tricyclic and tetracyclic aromatics is slightly higher for the experiments with water co-feed, in agreement with the TPD-TPO measurements. Since the duration of each experiment is different, we cannot rule out that the growth of polycyclic aromatics is favored with prolonged time on stream. Nevertheless, based on the fact that the deactivated catalysts reached a similar final conversion value, we can infer that the formation of polycyclic aromatics is favored at high water-to-methanol ratio values for the same conversion level. Our results also agree with those of Luo et al.,[42] who observed that the content of soluble species increases for the experiment with water co-feed in the oligomerization of olefins on a SAPO-34 catalyst. This may be indicative of the efficient use of the SAPO-18 crystals as previously mentioned in the TPD and TPO measurements and based on the observations of De Wispelaere et al.[51] for a SAPO-34 catalyst. This efficient use of the SAPO-18 crystals implies that more cavities are available for reactions leading to form more soluble retained species.

Figure 10b shows the abundance of the components of monocyclic aromatics for all the experiments. In general, the abundance of toluene, xylenes, tri-, tetra- and pentamethylbenzenes increases for the experiments with water co-feed. This verifies that co-feeding water favors the formation of more reactive monocyclic aromatic species at the same final conversion level, which is in line with the hypothesis of the efficient use of the SAPO-18 crystals.

#### 2.4.2.3. Analysis of Insoluble Species

The nature of the insoluble species (coke species insoluble in dichloromethane in the extract) was revealed using LDI FT-ICR/MS. Figure 11 shows the LDI FT-ICR/MS spectra of the three samples of insoluble coke formed in each experiment. The insoluble coke formed in all the experiments shows a narrow mass distribution in the range of 200–500 Da, whereas the insoluble coke formed with water co-feed shows a secondary broad mass distribution extended up to 1200 Da. All the spectra show increments of 14 Da in the m/z signals, which are assigned to $CH_2$ groups.[43] The spectra also reveal the presence of clusters according to the presence of narrow mass distributions. Thus, for the experiment without water co-feed, there is a cluster between 200 and 400 Da centered at 286 Da, which may comprise polycyclic aromatics containing around five or six aromatic rings in average with various degrees of alkylation. For the experiments with water co-feed, the insoluble coke shows two clusters, one similar to that observed for the experiment without water co-feed centered at 258 Da (polycyclic aromatics with five aromatic rings in average) and another centered at 353 Da (around six-seven aromatic rings). The difference in the maxima of these two clusters (95 Da) indicates an increment of an alkyl-substituted aromatic ring unit from one cluster to the next. These clusters of polycyclic aromatics are believed to grow up and remain retained in the cavities of the SAPO-18 crystals forming a sort of intracavity polycyclic aromatic structures.[43,44]

Remarkably, for the methanol-water feeds (Figure 11), the insoluble coke shows a very wide distribution in the 300–1200 Da interval, which indicates a prominent formation of polycyclic aromatics with large numbers of aromatic rings. Wang et al.[43] proved that this kind of growth can be obtained when the ionization power in the FT-ICR is high enough to produce unselective oligomerization. Thus, as the results of Figure 11 have been obtained using the same ionization power, we may well conclude that reactants and products during the reaction continuously polymerize in the presence of water at the same final conversion level. Large polycyclic aromatics form an amorphous coke mainly located on the outer surface of the SAPO-18 crystals and on the mesoporous matrix surface of the catalyst. The formation of this coke is mainly from olefins and its growth seems to be favored when co-feeding water because the catalyst lifetime is prolonged.[51] When comparing the amount of coke (Figure 9) and soluble species (Figure 2b, 5b and 10) retained in the catalyst using different amounts of

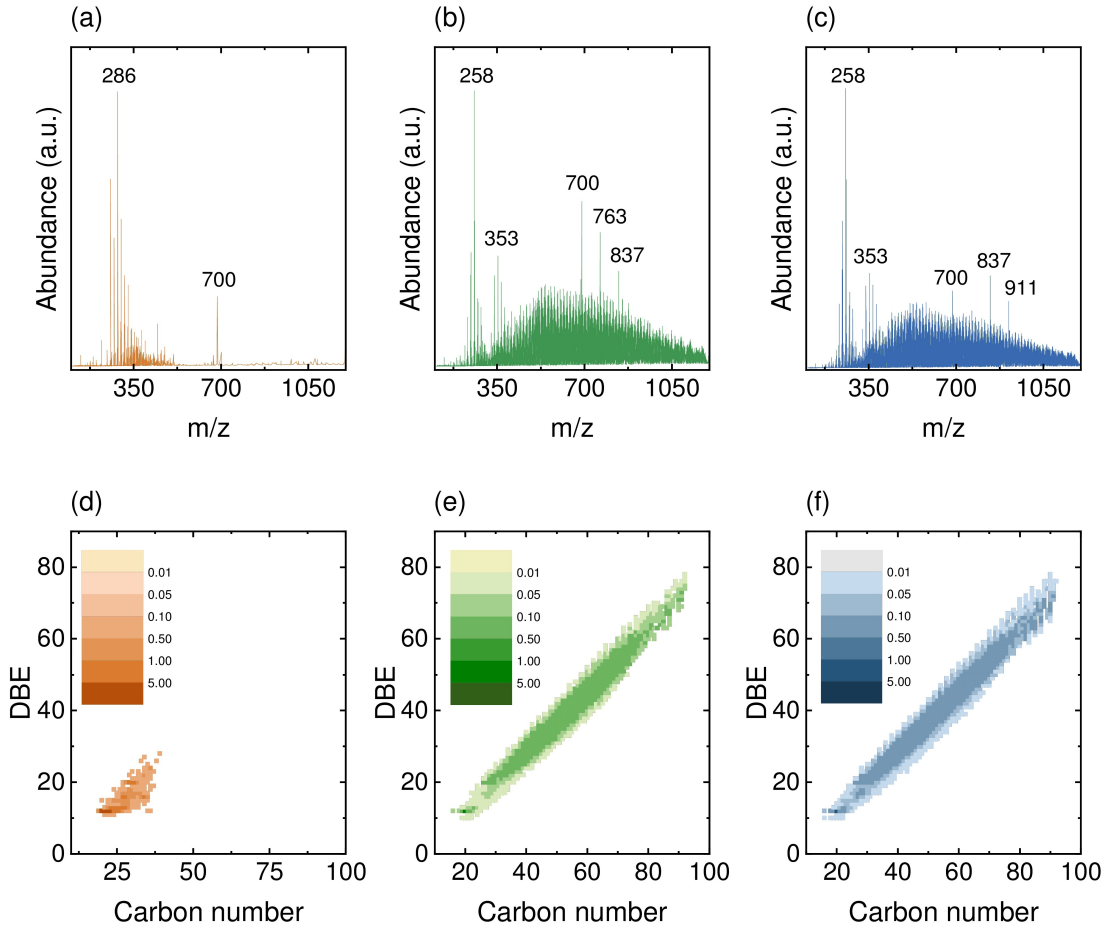


**Figure 11.** LDI FT-ICR/MS spectra and color-coded iso-abundance plots corresponding to the non-protonated CH species in the samples with different water-to-methanol ratio values in the feed: (a–d) $F_{W0}/F_{M0}=0$; (b–e) $F_{W0}/F_{M0}=0.11$; (c–f) $F_{W0}/F_{M0}=0.50$.

water (and final time on stream as shown in Figure 7) we can conclude that the amount of insoluble species is relatively low as compared to the total amount of retained species. However, the fact that we are able to detect these species indicate that water effectively helps the reactants, intermediates and products to diffuse through the crystal (lowering the reactivity of the acid sites), allowing the diffusion of these species toward the matrix material where they polymerize unselectively into heavy polycyclic aromatics. These observations are connected to the observations obtained from the experiments in the FTIR reactor, indicating that co-feeding water hinders the adsorption of olefins.

## 3. Conclusions

The use of different reactors with online monitoring of the products and retained species in the catalyst was satisfactory to study the effect of co-feeding water on the performance of the MTO reaction on a SAPO-18 catalyst. A differential reactor (UV-vis or FTIR cell reactors with low conversions) provided information on all the kinetic periods (induction-autocatalysis and deactivation) while an integral reactor (fixed-bed reactor with high conversions) provided information on the deactivation kinetics. As previously reported, the dynamics of the retained species are paramount for the MTO reaction, as they act as active (hydrocarbon pool) and deactivating (coke) species.

Our kinetic results point that, at any given moment (similar time on stream), co-feeding water leads to a decrease in the retained species in the catalyst. That is, decreasing the overall reaction rate or, conversely, decreasing the accessible acid sites for the reaction. What we proved using *in-situ* spectroscopy coupled with the online analysis of gaseous products in differential reactors is that the induction-autocatalysis and deactivation periods and the formation of all retained species are equally affected when co-feeding water. Thus, co-feeding water quenches equally the formation of active and deactivating species and this is closely related to quenching the induction-autocatalytic and deactivation periods. Another peculiar fact about co-feeding water is the effect on hindering the adsorption of olefins changing the nature of the retained species (mostly aromatic species).

At low conversions ($<20\%$), co-feeding water enhances the selectivity of light olefins, particular that of propylene, which may occur by the decrease in the density of acid sites for the adsorption of water that favors the reactions of the olefins cycle.

The lifetime of the catalyst can only be effectively measured in the conditions of the integral fixed-bed reactor, because we can keep a realistic concertation of species throughout the reaction. When this is the case, we proved that co-feeding water effectively enlarges the lifetime of the catalyst. This effect is due to (1) the quenching of deactivation as previously explained and (2) the diffusion of a very limited amount of retained species out of the SAPO-18 framework and the consecutive oligomerization-polymerization of these species on the matrix of the catalyst. We analyzed the nature of these polymerized species using high resolution mass spectrometry finding patterns and weights that correspond to this unselective oligomerization.

These observations prove that co-feeding water is a reliable strategy for controlling the acid site usage for the SAPO-18 catalyst during the MTO reaction. The degree of quenching promoted when co-feeding water is truly effective for extending the lifetime of the catalyst by diffusing olefins out of the SAPO-18 crystals. The removal of these olefins prevents the formation of aromatic species in the SAPO-18 crystals that limit the diffusion of products and reactants causing catalyst deactivation. However, olefins that are diffused out when co-feeding water promote the formation of polycyclic aromatics on the matrix surface (external coke) that does not cause significant deactivation as the aromatic species retained in the SAPO-18 cavities.

## Experimental Section

### Catalyst Preparation and Characterization

We synthetized a SAPO-18 zeotype by means of hydrothermal synthesis using the method of diisopropylethylamine (DPEA) as a template[70] and following the changes proposed by Álvaro-Muñoz et al.,[8] with the following gel composition:

$$Al_2O_3 : 0.8P_2O_5 : 0.6SiO_2 : 25H_2O : 1.6DPEA.$$

The reagents were $Al(OH)_3{\cdot}xH_2O$ (Sigma Aldrich, 100%), $H_3PO_4$ (Sigma Aldrich, 85%), fumed $SiO_2$ (Degussa, Aerosil), and N,N-diisopropylethylamine (Sigma-Aldrich, 99%). The synthesis procedure consisted of preparing and keeping in agitation a $H_3PO_4$ solution (6.8 M), and slowly adding $Al(OH)_3$, $SiO_2$ and the template stepwise. The crystallization of the resulting gel took place in a Teflon-lined stainless-steel autoclave vessel at 160 °C under autogenous pressure for 6 days. For the crystallization, we used seeds of SAPO-18 crystals provided by the group of Sastre.[8] We recovered the crystallization product by filtration, washing with ethanol and distilled water, drying at 110 °C for 24 h, and calcination at 550 °C for 3 h with a heating rate of 5 °C $min^{-1}$. In order to prepare the catalyst, we mixed 50 wt% of the resulting SAPO-18 zeotype with 30 wt% of pseudo-boehmite (Sasol, 70 wt% $\gamma$-alumina) and 20 wt% of $\alpha$-alumina (Alfa Aesar, colloidal dispersion at 20% in water). The procedure to obtain the catalyst particles consisted of drying the resulting wet mixture at room temperature for 24 h and at 110 °C for 24 h, followed by crushing and sieving to a size of 0.125–0.300 mm, and calcination at 550 °C for 2 h.

We characterized the SAPO-18 zeotype and catalyst using X-ray photoelectron spectroscopy (XPS), X-ray diffraction (XRD), solid-state $^{29}Si$ solid-state nuclear magnetic resonance ($^{29}Si$ NMR), $N_2$ physisorption, $NH_3$ adsorption and temperature-programmed desorption ($NH_3$-TPD), and Fourier-transform infrared (FTIR) spectroscopy. We followed the typical experimental procedures described in a previous publication.[40]

Additionally, we characterized the spent catalysts using temperature-programmed desorption (TPD) and oxidation (TPO) and extraction of soluble species. We performed the TPD-TPO measurements in a thermobalance (TA Instruments, Q5000), and the experimental procedure consisted of: (i) outgassing ~15 mg of

sample at 200 °C for 20 min in $N_2$ flow; (ii) heating at 10 °C min$^{-1}$ in 50 cm$^3$ min$^{-1}$ of $N_2$ up to 550 °C and holding for 1 h; (iii) cooling down to 200 °C and switching the flow to air at 50 cm$^3$ min$^{-1}$; and (iv) heating at 10 °C min$^{-1}$ up to 550 °C and holding for 90 min. The extraction of retained species is an adaptation of the procedure developed before.[40] The experimental procedure consisted of: (i) treating ~10 mg of sample in HF (Merck, 40%) with a sample/HF ratio of 10 cm$^3$ g$^{-1}$ in a Teflon container for 1 h; (ii) neutralizing with a NaOH (Panreac, pure) solution; (iii) adding 3 cm$^3$ of dichloromethane (Sigma-Aldrich, 99.8%) and shaking for 1 min; (iv) allowing to separate the organic (extract) and aqueous phases for 2 h and recovering the organic phase for analysis. The extract contains retained species that are soluble and insoluble in dichloromethane. We analyzed the organic phase (soluble species) in a gas chromatograph coupled with a mass spectrometer (Shimadzu, GCMS-QP2010S).

We studied the nature of insoluble species by means of laser desorption ionization (LDI) FT-ICR MS using a Bruker SolariX XR 9.4 Tesla FT-ICR MS Instrument (Bruker Daltonik GmbH, Bremen). The samples of insoluble coke were crushed on the MALDI sample plate. Laser power was set as "medium", with a 1000 Hz frequency and laser shots were 50. The laser power (18–28%) was adjusted individually for each sample in order to achieve high signals without obvious fragmentation. Data was recorded with the m/z range of 154–1200 Da, at the size of 8Megawords. The transient time for each scan was 4.4739 s, and 50 scans were accumulated to generate the final spectrum for each sample. The obtained spectra were processed using the Bruker DataAnalysis V4.5 software and the chemical formula assignment was conducted through Composer software (Sierra Analytics). The double bond equivalent (DBE) number of the $C_cH_hO_oN_nS_s$ molecule was defined by means of Equation 2.

$$DBE = c - \frac{h}{2} + 1 \tag{2}$$

### Experiments in UV-Vis and FTIR Cell Reactors

We carried out kinetic tests for the MTO reaction in UV-vis or FTIR cell reactors at the following constant conditions: temperature ($T$) = 400 °C; pressure ($P$) = 1.0 bar; methanol partial pressure ($P_{M0}$) = 0.014 bar; methanol flowrate ($F_{M0}$) = 0.012 mol h$^{-1}$; catalyst weight ($W$) = 0.012 g; space time ($W/F_{M0}$) = 1 g h mol$^{-1}$. The diluent was $N_2$ for the reference experiment (water-to-methanol ratio of $F_{W0}/F_{M0}$ = 0), whereas water was a co-diluent for the experiment with a water-to-methanol ratio of 0.50. The UV-vis cell reactor consisted of a commercial Linkam cell (THMS600 stage) coupled with a UV-vis spectrometer (Jasco, V-780) with a special compartment (Jasco, ARN-915i) for the cell. The FTIR cell reactor consisted of commercial Specac transmission cell (HPHT cell) coupled with a FTIR spectrometer (Thermo Scientific, Nicolet 6700). For both reactors, the feed consisted of $N_2$-containing methanol vapor or methanol and water vapors keeping constant the methanol partial pressure (water vapor partially replaces $N_2$). We obtained these vapors by flowing $N_2$ through saturator vessels containing methanol or water, and we calculated the methanol and water concentrations using the equilibrium data at 20 °C. We analyzed the effluent gas using a mass spectrometer (Pfeiffer Vacuum, Omnistar GSD 320 O Series) continuously measuring the m/z signals of 16, 18, 27, 29, 31, 41, 43, 45, 55, 56, 57, 78 and 91. We correlated the intensities of the m/z signals with a previous calibration using the micro-gas chromatograph and calculated the conversion and selectivity of products based on groups of light olefins (m/z = 41) and light paraffins + heavy aliphatics (m/z = 43, 55, 56 and 57). In the experiments carried out in the UV-vis cell reactor, we collected UV-vis spectra every 35 s for 4 h, with a measurement range of 250–850 nm at a scan speed of 4000 nm min$^{-1}$, UV-vis response of 0.24 s and data interval of 2 nm. In the experiments carried out in the FTIR cell reactor, we collected FTIR spectra every 2 min for 4 h with a measurement range of 1300–4000 cm$^{-1}$, resolution of 4 cm$^{-1}$ and 100 scans. We used Eqs. (2) and (4) for calculating the conversion and selectivity based on the online analysis of gaseous products.

### Experiments in a Fixed-Bed Reactor

We carried out the main kinetic tests for the MTO reaction in a conventional fixed-bed reactor at the following constant conditions: temperature ($T$) = 400 °C; pressure ($P$) = 1.85 bar; methanol partial pressure ($P_{M0}$) = 0.610 bar; methanol flowrate ($F_{M0}$) = 0.1 mol h$^{-1}$; catalyst weight ($W$) = 0.1 g; space time ($W/F_{M0}$) = 1 g h mol$^{-1}$. The diluent was He for the reference experiment (water-to-methanol ratio of $F_{W0}/F_{M0}$ = 0), whereas water was a co-diluent for the experiments with different water-to-methanol ratio values adjusted by feeding methanol-water mixtures. We described the reaction setup in a previous publication.[40] Briefly, the reactor is a stainless-steel tube (i.d. 9 mm) with a fixed-bed arrangement of 6 cm$^3$ consisting of a mixture of SiC (VWR Chemicals, < 0.105 mm) and catalyst sample. The reactor is inside a hot box kept at 200 °C to prevent the condensation of the products for analysis in gas-vapor phase. The feed consisted of liquid methanol or methanol-water mixtures pumped at 0.1 mol h$^{-1}$ of methanol, which is evaporated in the hot box, and carried with He at adjusted flowrates in order to keep the same methanol partial pressure (water partially replaces He as diluent). For the analysis of the effluent gas, we used an online micro-gas chromatograph (Varian, CP4900) with a thermal conductivity detector and three column channels for simultaneous analysis: (i) Molesieve 5A (fumed $SiO_2$, packed length = 8 m, column temperature = 45 °C, column injection temperature = 65 °C, column pressure = 26) for separation of $N_2$, $O_2$, CO and $CH_4$; (ii) PoraPLOT Q (packed length = 10 m, column temperature = 80 °C, column injection temperature = 80 °C, column pressure = 26 psi) for separation of $C_1$–$C_4$ hydrocarbons and oxygenates; and (iii) CP-Sil 5 CB (packed length = 10 m, column temperature = 80 °C, column injection temperature = 80 °C, column pressure = 26 psi) for separation of $C_4$–$C_{10}$ hydrocarbons and oxygenates.

We calculated the carbon-based conversion ($X$) assuming that all the identified oxygenates (methanol and dimethyl ether) are reactants as in Equation (3):

$$X = \frac{F_{M0} - F_M}{F_{M0}} = 1 - Y_M \tag{3}$$

where $F_{M0}$ is the carbon-based molar flowrate of oxygenates in the feed, $F_M$ is the carbon-based molar flowrate of oxygenates in the effluent gas, and $Y_M$ is the carbon-based yield of oxygenates in the effluent gas. We calculated the carbon-based yield of a product $i$ ($Y_i$) [Eq. (4)] or the carbon-based selectivity of a product $i$ ($S_i$) [Eq. (5)] as:

$$Y_i = \frac{F_i}{F_{M0}} \tag{4}$$

$$S_i = \frac{F_i}{F_{M0} - F_M} = \frac{Y_i}{X} \tag{5}$$

where $F_i$ is the carbon-based molar flowrate of product $i$.

## Abbreviations

| | |
|---|---|
| -CA | -cyclic aromatic(s) |
| FTIR | Fourier-transform infrared |
| LDI FT-ICR | laser-desorption-ionization Fourier-transform ion-cyclotron-resonance |
| -MB | -methylbezene(s) |
| MS | mass spectrometry |
| MTO | methanol-to-olefins |
| TPD | temperature-programed desorption |
| TPO | temperature-programed oxidation |
| UVvis | ultraviolet-visible |

## *Acknowledgment*

*This work was possible thanks to the financial support of the Ministry of Economy, Industry and Competitiveness of the Spanish Government (Project CTQ2016-79646-P, co-founded with ERDF funds), the Basque Government (Project IT748-13, IT912-16) and the King Abdullah University of Science and Technology (KAUST). J.V. is thankful for his fellowship granted by the Ministry of Economy, Industry and Competitiveness of the Spanish Government (BES-2014-069980). The authors are thankful for technical and human support provided by IZO-SGI SGIker of UPV/EHU and European funding (ERDF and ESF).*

## *Conflict of Interest*

The authors declare no conflict of interest.

**Keywords:** coke deactivation · high-resolution mass spectrometry · *in-situ* spectroscopy · methanol-to-hydrocarbons (MTH) reaction · SAPO-18 (AEI) zeolite

[1] P. Tian, Y. Wei, M. Ye, Z. Liu, *ACS Catal.* **2015**, *5*, 1922–1938.
[2] A. Galadima, O. Muraza, *Ind. Eng. Chem. Res.* **2015**, *54*, 4891–4905.
[3] J. Lefevere, S. Mullens, V. Meynen, J. Van Noyen, *Chem. Pap.* **2014**, *68*, 1143–1153.
[4] M. Yang, D. Fan, Y. Wei, P. Tian, Z. Liu, *Adv. Mater.* **2019**, *31*, 1–15.
[5] Z. Li, J. Martínez-Triguero, J. Yu, A. Corma, *J. Catal.* **2015**, *329*, 379–388.
[6] M. Hunger, M. Seiler, A. Buchholz, *Catal. Lett.* **2001**, *74*, 61–68.
[7] M. A. Ali, S. Ahmed, N. Al-Baghli, Z. Malaibari, A. Abutaleb, A. Yousef, *Catal. Lett.* **2019**, *149*, 3395–3424.
[8] T. Álvaro-Muñoz, C. Márquez-Álvarez, E. Sastre, *Top. Catal.* **2016**, *59*, 278–291.
[9] A. T. Aguayo, A. G. Gayubo, R. Vivanco, M. Olazar, J. Bilbao, *Appl. Catal. A* **2005**, *283*, 197–207.
[10] A. G. Gayubo, R. Vivanco, A. Alonso, B. Valle, A. T. Aguayo, *Ind. Eng. Chem. Res.* **2005**, *44*, 6605–6614.
[11] J. Chen, J. M. Thomas, P. A. Wright, R. P. Townsend, *Catal. Lett.* **1994**, *28*, 241–248.
[12] R. Martínez-Franco, Z. Li, J. Martínez-Triguero, M. Moliner, A. Corma, *Catal. Sci. Technol.* **2016**, *6*, 2796–2806.
[13] M. A. Djieugoue, A. M. Prakash, L. Kevan, *J. Phys. Chem. B* **2000**, *104*, 6452–6461.
[14] S. Gao, Z. Liu, S. Xu, A. Zheng, P. Wu, B. Li, X. Yuan, Y. Wei, Z. Liu, *J. Catal.* **2019**, *377*, 51–62.
[15] I. Pinilla-Herrero, U. Olsbye, C. Márquez-Álvarez, E. Sastre, *J. Catal.* **2017**, *352*, 191–207.
[16] S. Ilias, A. Bhan, *ACS Catal.* **2013**, *3*, 18–31.
[17] C. M. Wang, Y. D. Wang, H. X. Liu, G. Yang, Y. J. Du, Z. K. Xie, *Cuihua Xuebao/Chinese J. Catal.* **2015**, *36*, 1573–1579.
[18] J. Chen, J. Li, C. Yuan, S. Xu, Y. Wei, Q. Wang, Y. Zhou, J. Wang, M. Zhang, Y. He, S. Xu, Z. Liu, *Catal. Sci. Technol.* **2014**, *4*, 3268–3277.
[19] A. Hwang, B. A. Johnson, A. Bhan, *J. Catal.* **2019**, *369*, 86–94.
[20] A. G. Gayubo, A. T. Aguayo, A. Alonso, J. Bilbao, *Ind. Eng. Chem. Res.* **2007**, *46*, 1981–1989.
[21] D. Chen, A. Grønvold, K. Moljord, A. Holmen, *Ind. Eng. Chem. Res.* **2007**, *46*, 4116–4123.
[22] P. Cnudde, R. Demuynck, S. Vandenbrande, M. Waroquier, G. Sastre, V. Van Speybroeck, *J. Am. Chem. Soc.* **2020**, *142*, 6007–6017.
[23] U. Olsbye, S. Svelle, K. P. Lillerud, Z. H. Wei, Y. Y. Chen, J. F. Li, J. G. Wang, W. B. Fan, *Chem. Soc. Rev.* **2015**, *44*, 7155–7176.
[24] W. Dai, G. Wu, L. Li, N. Guan, M. Hunger, *ACS Catal.* **2013**, *3*, 588–596.
[25] R. B. Rostami, M. Ghavipour, Z. Di, Y. Wang, R. M. Behbahani, *RSC Adv.* **2015**, *5*, 81965–81980.
[26] D. Chen, K. Moljord, A. Holmen, *Microporous Mesoporous Mater.* **2012**, *164*, 239–250.
[27] S. Gao, S. Xu, Y. Wei, Q. Qiao, Z. Xu, X. Wu, M. Zhang, Y. He, S. Xu, Z. Liu, *J. Catal.* **2018**, *367*, 306–314.
[28] A. Hwang, T. T. Le, Z. Shi, H. Dai, J. D. Rimer, A. Bhan, *J. Catal.* **2019**, *369*, 122–132.
[29] J. F. Haw, D. M. Marcus, *Top. Catal.* **2005**, *34*, 41–48.
[30] M. Guisnet, *J. Mol. Catal. A* **2002**, *182–183*, 367–382.
[31] K. Hemelsoet, Q. Qian, T. De Meyer, K. De Wispelaere, B. De Sterck, B. M. Weckhuysen, M. Waroquier, V. Van Speybroeck, *Chem. A Eur. J.* **2013**, *19*, 16595–16606.
[32] D. Mores, E. Stavitski, M. H. F. Kox, J. Kornatowski, U. Olsbye, B. M. Weckhuysen, *Chem. A Eur. J.* **2008**, *14*, 11320–11327.
[33] Q. Qian, J. Ruiz-Martínez, M. Mokhtar, A. M. Asiri, S. A. Al-Thabaiti, S. N. Basahel, H. E. Van der Bij, J. Kornatowski, B. M. Weckhuysen, *Chem. A Eur. J.* **2013**, *19*, 11204–11215.
[34] E. Borodina, H. Sharbini Harun Kamaluddin, F. Meirer, M. Mokhtar, A. M. Asiri, S. A. Al-Thabaiti, S. N. Basahel, J. Ruiz-Martinez, B. M. Weckhuysen, *ACS Catal.* **2017**, *7*, 5268–5281.
[35] J. F. Haw, W. Song, D. M. Marcus, J. B. Nicholas, *Acc. Chem. Res.* **2003**, *36*, 317–326.
[36] E. Borodina, F. Meirer, I. Lezcano-González, M. Mokhtar, A. M. Asiri, S. A. Al-Thabaiti, S. N. Basahel, J. Ruiz-Martinez, B. M. Weckhuysen, *ACS Catal.* **2015**, *5*, 992–1003.
[37] Q. Qian, J. Ruiz-Martínez, M. Mokhtar, A. M. Asiri, S. A. Al-Thabaiti, S. N. Basahel, B. M. Weckhuysen, *Catal. Today* **2014**, *226*, 14–24.
[38] X. Zhu, J. P. Hofmann, B. Mezari, N. Kosinov, L. Wu, Q. Qian, B. M. Weckhuysen, S. Asahina, J. Ruiz-Martínez, E. J. M. Hensen, *ACS Catal.* **2016**, *6*, 2163–2177.
[39] W. Dai, X. Wang, G. Wu, L. Li, N. Guan, M. Hunger, *ChemCatChem* **2012**, *4*, 1428–1435.
[40] J. Valecillos, E. Epelde, J. Albo, A. T. Aguayo, J. Bilbao, P. Castaño, *Catal. Today* **2020**, *348*, 243–256.
[41] J. Zhou, Y. Zhi, J. Zhang, Z. Liu, T. Zhang, Y. He, A. Zheng, M. Ye, Y. Wei, Z. Liu, *J. Catal.* **2019**, *377*, 153–162.
[42] M. Luo, Y. Fu, B. Hu, D. Wang, B. Wang, G. Mao, *Appl. Catal. A* **2019**, *570*, 209–217.
[43] N. Wang, Y. Zhi, Y. Wei, W. Zhang, Z. Liu, J. Huang, T. Sun, S. Xu, S. Lin, Y. He, A. Zheng, Z. Liu, *Nat. Commun.* **2020**, *11*, DOI 10.1038/s41467-020-14493–9.
[44] M. Gao, H. Li, W. Liu, Z. Xu, S. Peng, M. Yang, M. Ye, Z. Liu, *Nat. Commun.* **2020**, *11*, 3641.
[45] M. R. Gogate, *Pet. Sci. Technol.* **2019**, *37*, 559–565.
[46] F. J. Keil, *Microporous Mesoporous Mater.* **1999**, *29*, 49–66.
[47] S. Xu, Y. Zhi, J. Han, W. Zhang, X. Wu, T. Sun, Y. Wei, Z. Liu, in *Adv. Catal.*, Elsevier Inc., **2017**, pp. 37–122.
[48] M. Stöcker, in *Zeolites Catal.*, Wiley-VCH Verlag GmbH & Co. KGaA, Weinheim, Germany, **2010**, pp. 687–711.
[49] A. G. Gayubo, A. T. Aguayo, A. Alonso, A. Atutxa, J. Bilbao, *Catal. Today* **2005**, *106*, 112–117.
[50] A. J. Marchi, G. F. Froment, *Appl. Catal.* **1991**, *71*, 139–152.
[51] K. De Wispelaere, C. S. Wondergem, B. Ensing, K. Hemelsoet, E. J. Meijer, B. M. Weckhuysen, V. Van Speybroeck, J. Ruiz-Martínez, *ACS Catal.* **2016**, *6*, 1991–2002.
[52] R. Wendelbo, D. Akporiaye, A. Andersen, I. M. Dahl, H. B. Mostad, *Appl. Catal. A* **1996**, *142*, 197–207.
[53] P. Pérez-Uriarte, M. Gamero, A. Ateka, M. Díaz, A. T. Aguayo, J. Bilbao, *Ind. Eng. Chem. Res.* **2016**, *55*, 1513–1521.

[54] A. T. Aguayo, A. G. Gayubo, R. Vivanco, A. Alonso, J. Bilbao, *Ind. Eng. Chem. Res.* **2005**, *44*, 7279–7286.
[55] W. Dai, C. Wang, M. Dyballa, G. Wu, N. Guan, L. Li, Z. Xie, M. Hunger, *ACS Catal.* **2015**, *5*, 317–326.
[56] A. G. Gayubo, A. T. Aguayo, A. L. Morán, M. Olazar, J. Bilbao, *AIChE J.* **2002**, *48*, 1561–1571.
[57] A. D. Chowdhury, K. Houben, G. T. Whiting, M. Mokhtar, A. M. Asiri, S. A. Al-Thabaiti, S. N. Basahel, M. Baldus, B. M. Weckhuysen, *Angew. Chem. Int. Ed.* **2016**, *55*, 15840–15845; *Angew. Chem.* **2016**, *128*, 16072–16077.
[58] X. Wu, S. Xu, W. Zhang, J. Huang, J. Li, B. Yu, Y. Wei, Z. Liu, *Angew. Chem. Int. Ed.* **2017**, *56*, 9039–9043; *Angew. Chem.* **2017**, *129*, 9167–9171.
[59] J. Valecillos, J. Ruiz-Martinez, A. T. Aguayo, P. Castaño, *Chem. A Eur. J.* **2020**, DOI 10.1002/chem.202004865.
[60] A. Mehdad, N. Gould, B. Xu, R. Lobo, *Catal. Sci. Technol.* **2017**, *8*, 358–366.
[61] D. Rojo-Gama, M. Signorile, F. Bonino, S. Bordiga, U. Olsbye, K. P. Lillerud, P. Beato, S. Svelle, *J. Catal.* **2017**, *351*, 33–48.
[62] E. Epelde, M. Ibáñez, J. Valecillos, A. T. Aguayo, A. G. Gayubo, J. Bilbao, P. Castaño, *Appl. Catal. A* **2017**, *547*, 176–182.
[63] S. Bailleul, S. M. J. Rogge, L. Vanduyfhuys, V. Van Speybroeck, *ChemCatChem* **2019**, *11*, 3993–4010.
[64] L. Marchese, J. Chen, P. A. Wright, J. M. Thomas, *J. Phys. Chem.* **1993**, DOI 10.1021/j100133a001.
[65] J. Valecillos, G. Elordi, A. T. Aguayo, P. Castaño, *Catal. Sci. Technol.* **2021**, *11*, 1269–1281.
[66] G. Qi, Z. Xie, W. Yang, S. Zhong, H. Liu, C. Zhang, Q. Chen, *Fuel Process. Technol.* **2007**, *88*, 437–441.
[67] D. M. Marcus, W. Song, L. L. Ng, J. F. Haw, *Langmuir* **2002**, *18*, 8386–8391.
[68] H. G. Jang, H. K. Min, J. K. Lee, S. B. Hong, G. Seo, *Appl. Catal. A* **2012**, *437–438*, 120–130.
[69] W. Song, H. Fu, J. F. Haw, *J. Am. Chem. Soc.* **2001**, *123*, 4749–4754.
[70] W. M. Meier, in *Verif. Synth. Zeolitic Mater.*, Elsevier, **2001**, pp. 81–83.

Manuscript received: January 25, 2021
Revised manuscript received: March 16, 2021
Accepted manuscript online: April 19, 2021
Version of record online: May 18, 2021